THE JOURNAL OF PHYSICAL CHEMISTRY C

Article

pubs.acs.org/JPCC

Enhanced Hydrate Nucleation near the Limit of Stability

Felipe Jiménez-Ángeles[†] and Abbas Firoozabadi*[,†,‡]

[†]Reservoir Engineering Research Institute, Palo Alto, California 94301, United States

[‡]Department of Chemical and Environmental Engineering, Yale University, New Haven, Connecticut 06510, United States

Supporting Information

ABSTRACT: Clathrate hydrates are crystalline structures composed of small guest molecules trapped into cages formed by hydrogen-bonded water molecules. In hydrate nucleation, water and the guest molecules may stay in a metastable fluid mixture for a long period. Metastability is broken if the concentration of the guest is above a certain limit. Here we study propane hydrates by means of molecular dynamics simulations. First we simulate three-phase equilibrium of water, propane, and propane hydrates; the simulated melting temperature and solubility of propane in water are agreement with experimental measurements. In the main part we simulate hydrate nucleation in water−propane supersaturated solutions. At moderate temperatures we show that hydrate nucleation can be very fast in a very narrow range of composition, namely, close to the limit of stability. Propane density fluctuations near the fluid−fluid demixing are coupled with crystallization, producing enhanced nucleation rates. This is the first report of propane-hydrate nucleation by molecular dynamics simulations. We observe motifs of the crystalline structure II in line with experiments and new hydrate cages not reported in the literature. Our study relates nucleation to the fluid−fluid spinodal decomposition and demonstration that the enhanced nucleation phenomenon is more general than short-range attractive interactions as suggested in nucleation of proteins.

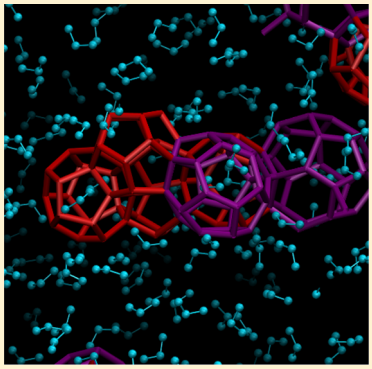

INTRODUCTION

Crystallization is a physical phase transition in many biological, industrial, and natural processes. Nucleation is the process during which a sufficiently large piece of crystal forms and begins to grow. Clathrate hydrates are ice-like structures made up of water-forming cages wherein some small molecules are hosted.[1,2] Small hydrocarbon molecules, nitrogen, carbon dioxide, and hydrogen sulfide, are some of the molecules forming hydrates. The most common structures of clathrate hydrates are structure I (sI), structure II (sII), and structure H (sH). The structure and stability conditions (P, T) of clathrate hydrates are affected by the guest molecule. The interest in hydrates spans over several areas of science and technology, among them geology, planetary and marine sciences, separation and sequestration processes, fuel transportation, climate change, and hydrogen storage.[3−9]

The nucleation mechanisms of crystallization are not fully resolved as they cannot be accessed experimentally. As a random phenomenon, nucleation time can be very long. A driving force is required to produce nucleation.[10,11] Low temperature, high pressure, and high supersaturation (excess of solute in the solution) increase the driving force and prompt hydrate formation.[12−14] In crystallization of proteins, the experiments[15,16] and coarse-grain molecular dynamics simulations[17,18] indicate that nucleation is accelerated close to the fluid−fluid demixing condition. Enhanced nucleation rates have been suggested to be related to proteins interacting through a short-range attractive potential based on coarse-grain simulations.[17−19]

Molecular dynamics simulations (MD) are employed for investigating clathrate hydrate nucleation at different conditions in different guest molecules.[12−14,20−28] Attempts to simulate propane hydrate nucleation have been unsuccessful.[29] Using a coarse-grain model of water, Jacobson et al. observe face-sharing empty 5^{12} cages similar to the sII structure of propane hydrates.[25] MD simulations of hydrate nucleation are typically carried out at low temperature, high pressure, and high supersaturation. In spite of many advances, formation of unit cells of hydrate structures has been observed in a limited number of simulations.[13,14,30] Among alkanes, only MD simulations of methane hydrates have been reported. Much of the discussion in hydrate simulations is on the mechanisms leading to clathrate hydrate structures. Hydrate structures are difficult to predict in MD simulations because the systems are driven into arrested states. The long computational time may be a limitation in MD simulations.

Here we study hydrate nucleation and the three-phase equilibrium of water and propane using MD simulations. The paper is organized as follows: In the next section we present our models and we outline the setups employed to simulate the three-phase equilibrium and hydrate nucleation. In the following section, we discuss our main findings, and finally our conclusions are given in the closing part.

Received: February 25, 2015
Revised: March 27, 2015

DOI: 10.1021/acs.jpcc.5b01869
J. Phys. Chem. C XXXX, XXX, XXX−XXX

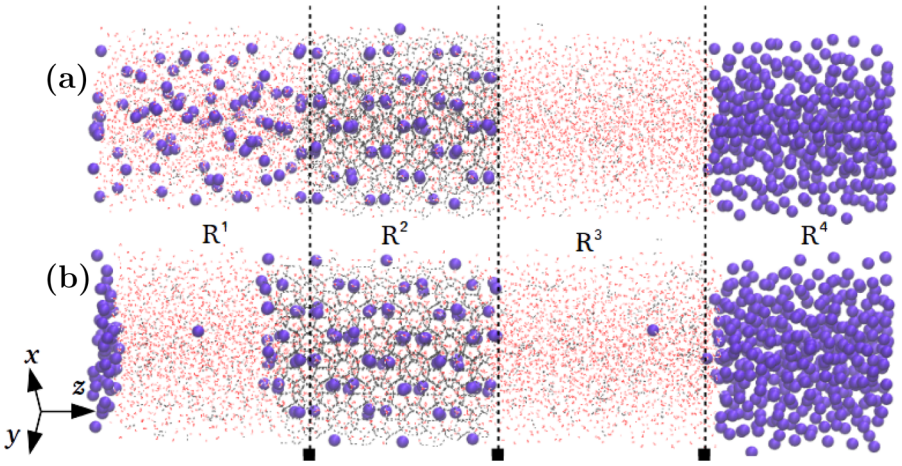

Figure 1. Snapshots of the setup used to establish the equilibrium conditions of water and propane models in three-phase systems. (a) $t = 0$ and (b) $t = 120$ ns. For clarity only the central atoms of propane molecules are shown (spheres); water molecules are shown in red and hydrogen bonds are shown as black lines.

MODELS AND METHODS

The TIP4P-ice model is used for water[31] whereas propane is represented by the united atom model.[32] Water molecules interact through long-range electrostatic forces (due to the partial charges of oxygen and hydrogen atoms) and van der Waals forces. Propane molecules interact only through van der Waals forces because their atoms do not have explicit partial charges. van der Waals interactions are taken into account by the Lennard-Jones potential and the atoms in molecules are held together by constraints. The Lorentz−Berthelot combining rules are used for cross water−propane interactions. Equations of motion are integrated using the leapfrog algorithm with a time-step of 2 fs and applying periodic boundary conditions. Long-range electrostatic interactions are computed using the smooth particle mesh Ewald summation; short-range interactions are truncated at a cutoff distance of 1.2 nm. The temperature is kept constant by means of the Nosé−Hoover thermostat with a relaxation time of $\tau_T = 2$ ps and pressure is kept constant by means of the Parrinello−Rahman barostat with a relaxation time of $\tau_P = 4$ ps. We use the open source code Gromacs[33] to carry out our simulations.

Equilibrium concentration is established when there are no net flows of mass and energy among different phases in contact. Hydrate nucleation is unlikely to occur in water-propane solutions at their equilibrium concentration. To produce hydrate nucleation, an unbalance of thermodynamic forces must exist.[10,11] Supersaturation of water−propane solutions are the unbalancing driving forces in our studies of hydrate nucleation. Solutions having concentrations above the equilibrium value are said to be supersaturated and are metastable. The limit of stability x_p^s is the maximum concentration of propane in a supersaturated solution and is mathematically defined by the condition $(\partial f_p/\partial x_p)|_{xp = x_p^s} = 0$, where f_p is the fugacity of propane in the mixture and x_p is the mole fraction of propane.[34] We first compute the equilibrium concentration and the limit of stability by means of the CPA equation-of-state.[35] At $T = 273.15$ K and $P = 500$ bar the equilibrium concentration of propane in water from CPA is $x_p^{eq} = 2 \times 10^{-4}$ whereas the limit of stability is $x_p^s = 0.043$.

To establish three-phase fluid−fluid−hydrate equilibrium, different setups are employed in the literature.[36−38] We use the setup shown in Figure 1a consisting of a prismatic rectangular simulation box divided in four regions. (1) In region R^1 there is a supersaturated aqueous solution made of 96 propane molecules and 1705 water molecules. (2) Region R^2 consists of a hydrate crystal slab built of $2 \times 2 \times 2$ unit cells of sII hydrate formed by 1632 water molecules and 96 propane molecules; the small 5^{12}-cages from the hydrate are empty whereas the large $5^{12}6^4$-cages are occupied by propane molecules. (3) Region R^3 is composed of 2045 water molecules. (4) Region R^4 contains 396 propane molecules. The initial dimensions of the four regions are $l_z^{(1)} = l_z^{(2)} = l_z^{(3)} = 5.2$ nm, and $l_z^{(4)} = 3$ nm in the z direction and $l_x = l_y = 3.46$ nm along the x and y directions. Periodic boundary conditions are applied in the three directions. A 200 ps MD simulation at $T = 200$ K and $P = 500$ bar is carried out to stabilize the system, followed by a temperature rise to $T = 270$ K carried out in seven MD simulations of 20 ps and temperature increments of 10 K between successive simulations. Further simulations at temperatures of 270, 275, 277, 280, and 285 K are carried out, followed by productions runs of 200 ns.

To investigate propane hydrate nucleation, we randomly place N_p propane molecules and N_w water molecules in a cubic box of initial side length l; the propane mole fraction is $x_p = N_p/N_w$. Details of the number of molecules employed in our simulations and initial lengths of the simulation boxes are provided in the Supporting Information. The overlapping of particles at the initial configuration is prevented by distance and energy criteria. A 3 ns simulation is carried out to stabilize the system at the target temperature T and pressure P. The resulting configuration is taken as the initial condition in the production run, which is monitored for hydrate formation. The stabilization and production runs are carried out at the same T and P. We set $P = 500$ bar in all of our simulations. A similar procedure has been employed to simulate methane hydrate nucleation.[14] Our simulations are carried out close to the limit of stability x_p^s. On the basis of our results from CPA equation-of-state we use $x_p = 0.045$ as the starting concentration in our simulations of nucleation. From here several conditions are tested to arrive to the optimal conditions.

RESULTS

To investigate the equilibrium properties of our water and propane models, we conduct simulations of the four-region

DOI: 10.1021/acs.jpcc.5b01869
J. Phys. Chem. C XXXX, XXX, XXX−XXX

setup at T = 270, 275, 280, 283, and 285 K. At T = 270 and 275 K we observe that the hydrate crystal slab grows whereas the propane concentration in the supersaturated solution (R^1) decreases. Figure 1 shows two snapshots of the simulation box at T = 275 K. Figure 1a is an snapshot at t = 0 and shows the supersaturated propane solution in region R^1, the initial thickness of crystal slab in region R^2, the aqueous phase with no dissolved propane in region R^3, and the propane phase in region R^4. Figure 1b is an snapshot at t = 120 ns and shows a drastic decrease of propane concentration in region R^1. The diffusion of some propane molecules to the right results in a thicker crystal slab; the outermost row of cages at the left-hand side of the slab is new and the cages at the inner row are totally formed. The growth of the crystal decreases as the propane concentration in region R^1 decreases and equilibrium is reached when hydrate growth stops. Note that in region R^1 most of propane molecules have moved to the left, indicating the low solubility of propane in water. In region R^1 the average numbers of water molecules and propane molecules in the aqueous solution are $\bar{N}_w$ = 1317 and $\bar{N}_p$ = 1.9, respectively; in the crystal region $\bar{N}_p$ = 113 and $\bar{N}_w$ = 2015, in region R^3 $\bar{N}_w$ = 2050 and $\bar{N}_p$ = 0.72, and in the propane phase $\bar{N}_p$ = 473. The equilibrium propane concentrations at each side of the crystal slab are $x_p = 1.4 \times 10^{-3}$ and $x_p = 3.4 \times 10^{-4}$, which are within the range of the reported experimental values.[39]

From $T \geq 280$ K the crystal slab melts (not shown): At 280 K the melting rate is such that two propane molecules detach from the crystal in 200 ns, at T = 283 K two molecules detach from the crystal slab in about 120 ns, and at 285 K the crystal is clearly melting. The slow melting rate of hydrates near the equilibrium temperature has been pointed out by Michalis et. al.[38] On the basis of our simulations the melting temperature is estimated at $T_m = 277.5 \pm 2.5$ K, which is close to the reported experimental value of $T_m \approx 278$ K.[40] Next we investigate propane hydrate nucleation.

Figure 2 shows potential energy vs simulation time of four simulation setups with slightly different propane concentrations but vastly different results. The potential energy of the system with mole fraction x_p = 0.045 fluctuates around a constant value over a time of more than 500 ns (light blue line), implying that the system remains in a metastable stationary state. For x_p = 0.048 the potential energy stays around a constant value during the initial stages and begins to decrease quickly at around $t \approx$ 48 ns. At this time hydrate growth initiates. The growth period is the relaxation time of the system from the nucleation time to equilibrium. The lowest value of the potential energy is reached at $t \approx$ 550 ns. The potential energy for x_p = 0.049 starts to decrease at $t \approx$ 45 ns of simulations and does not have large variations from $t \approx$ 450 ns. The potential energy for x_p = 0.050 increases sharply, implying that the mixture separates into propane and water liquid phases. The nucleation time τ_n may be defined around the time when the potential energy drops below the constant energy reference line. It can be determined when the horizontal reference line and the sloped line intersect in Figure 2.

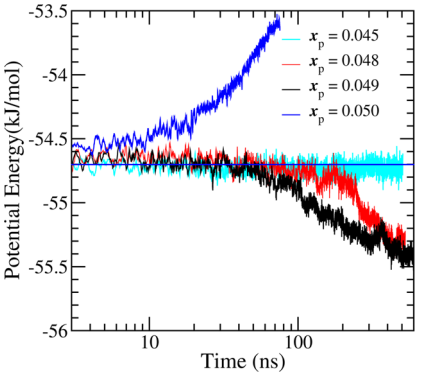

Figure 2. Potential energy vs time for four systems with different propane concentrations. The simulations boxes are prepared with N_w = 6600 water molecules and N_p = 312, 332, 342, 352 propane molecules corresponding to the propane mole fractions of x_p = 0.045, 0.048, 0.049, and 0.050, respectively. A horizontal reference line is drawn to guide the eye through the average constant values of energy based on x_p = 0.045; T = 273.15 K, and P = 500 bar.

As nucleation is a stochastic process, we use independent trajectories to compute the nucleation time at each composition (Table S1 in the Supporting Information). We carry out a number of duplicate simulations at T = 270.15, 273.15, and 275.15 K. At T = 275.15 K there is not hydrate nucleation in simulation runs of 500 ns. Figure 3 portrays the nucleation time as a function of the mole fraction of propane x_p at T = 270.15 and 273.15 K. At T = 270.15 K a decreasing trend of the nucleation time as a function of the propane concentration is observed within the composition interval of $0.041 \geq x_p \leq 0.05$. At T = 273.15 K we observe that $\tau_n(x_p=0.048) > \tau_n(x_p=0.049)$; there is a very narrow range in which hydrate nucleation occurs. For comparable concentrations at the two different temperatures, the nucleation time is shorter at T = 270.15 K than at T = 273.15. That is, as the temperature decreases, the driving force increases and the nucleation time decreases.[10] Outside these concentration intervals nucleation is not observed in simulation runs of 500 ns. From our MD simulations the water−propane limit of stability is established at x_p^s = 0.049 for T = 273.15 K and at x_p^s = 0.05 for T = 270.15 K. These values are in good agreement with the prediction of the CPA equation of state of 0.043 at T = 273.15 K. For concentrations above the limit of stability, the mixture separates.

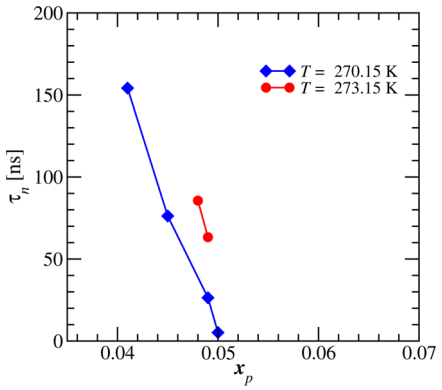

Figure 3. Nucleation time, τ_n, in nanoseconds as a function of the propane mole fraction at T = 270.15 and 273.15 K; P = 50 bar (Table S1 in the Supporting Information).

We stop all of our simulations when the hydrate growth rate becomes slow due to the decrease in the driving force. In one of the simulation runs the initial (total) propane concentration in the liquid phase is x_p = 0.048. At $t \approx$ 550 ns the propane concentration in the liquid phase is $x_p \approx 0.016$, and decreases to $x_p \approx 0.013$ at 2 μs. As we mention in the equilibrium

DOI: 10.1021/acs.jpcc.5b01869
J. Phys. Chem. C XXXX, XXX, XXX−XXX

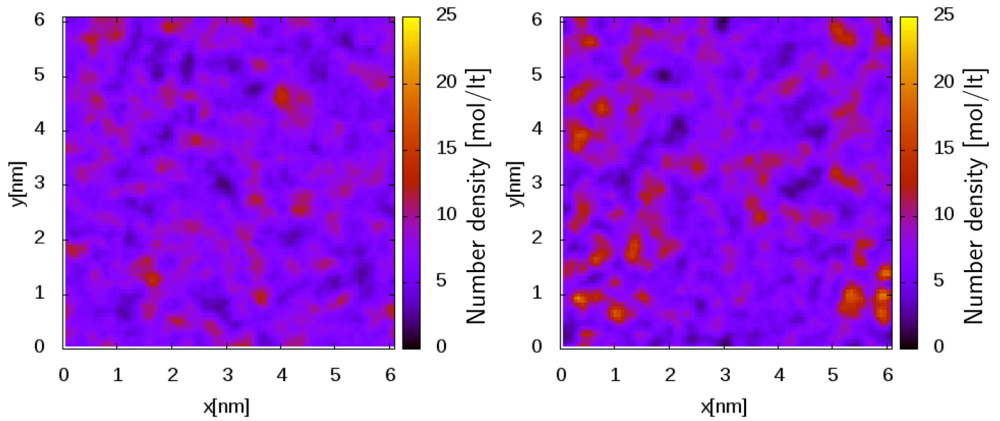

Figure 4. Propane 2D-density profile in the simulation box averaged over an interval of 10 ns for (a) $x_p = 0.045$ and (b) $x_p = 0.048$. In both cases the density profile is calculated in the simulation interval of 70 to 80 ns, $T = 273.15$ K, and $P = 500$ bar. The nucleation time for the simulation run at $x_p = 0.048$ is $\tau_n = 95$ ns. Lower densities are toward the blue whereas higher densities are reddish.

simulations at $T = 273.15$ K and $P = 500$ bar, the solubility of propane in water is about $x_p = 6 \times 10^{-4}$. In our nucleation simulations, a much longer simulation time is probably needed to reach the equilibrium concentration.

To investigate the correlation between phase demixing and hydrate nucleation enhancement, we compare the propane density fluctuations at two different concentrations of $x_p = 0.045$ and $x_p = 0.048$ both at $T = 273.15$ K and $P = 500$ bar. Nucleation is not observed for the lower concentration whereas nucleation is always produced for the higher concentration (in three independent runs presented in the Supporting Information). The 2D-density profiles are computed over a 100×100 uniform grid in the $x-y$ directions and averaged over 1000 configurations in a 10 ns interval (Figure 4). The time interval is selected from 70 to 80 ns. In this time interval there is no hydrate nucleation at $x_p = 0.048$. It is seen that, as propane concentration increases, the tendency of the two components to separate produces greater density fluctuations. Our results exhibit a relationship between density fluctuations and the nucleation induction time; the greater the density fluctuations, the smaller the induction time. Higher density fluctuations in the limit of stability and criticality of fluid–fluid systems is well established.[41] Our observation is in line with the fact that during the initial stages of methane hydrate nucleation several methane molecules surround and stabilize the first cage.[22] With greater propane density fluctuations the probability of formation of the first stable cage increases.

Hydrate growth is investigated by following the size of the clusters formed. To calculate the cluster size, we search for all the pentagonal faces formed by connected oxygen atoms. Two oxygen atoms are connected if they are within a distance of 0.35 nm. Two faces are connected if they share at least one water molecule. The size of a cluster N_5 is equal to the number of connected faces. A pentagonal face can be part of only one cluster. Figure 5 shows the evolution of the cluster size N_5 as a function of time for the two largest clusters formed in one of the simulation trajectories for $x_p = 0.048$. At $t \approx 30$ ns the largest cluster starts to grow and reaches a value of ≈ 60 pentagonal faces and decreases for a short time. From $t \approx 50$ ns the sustained growth of the largest cluster initiates. The large fluctuations in the cluster size are probably related to the fact that the hydrate structure formed is not in the lowest energy state. Through configuration changes the system explores

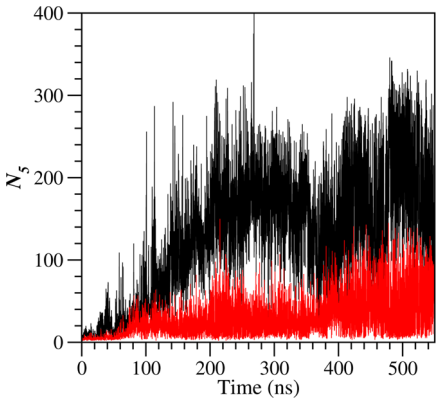

Figure 5. Instantaneous size of the two largest clusters in the simulation box during hydrate nucleation and growth. The cluster size N_5 is defined as the number of connected pentagonal rings. $N_w = 6600$, $N_p = 332$ ($x_p = 0.048$), $T = 273.15$ K, and $P = 500$ bar. The nucleation time is $\tau_n = 48$ ns.

different energy states. The lowest energy configuration is probably reached in a different scale of time.

In the simulations that do not proceed to hydrate growth (e.g., $x_p = 0.045$), around 10 unsuccessful nucleation events are observed within a simulation time of 500 ns. The cluster size can reach a size up to $N_5 \approx 30$, remains stable only for 2 ns, and disappears. Sarupria and Debenedetti calculate the cluster size based on the tetrahedral parameter q.[28] For propane hydrates we observe a strong dependence of the selected structure on q (Figure S2 in the Supporting Information). Our proposed parameter N_5 unambiguously accounts for hydrate structures.

To further characterize our simulation results, we classify the geometry of the cages formed following a standard procedure.[14,23] The geometry of the most abundant cages found in our simulation are shown in the inset of Figure 6a. Empty cages are $4^3 5^6$, $4^2 5^8$, and 5^{12} whereas the filled cages are $5^{12}6^2$, $5^{12}6^3$, and $5^{12}6^4$. The $5^{12}6^2$ cage is specific to structure sI in a ratio of 6:2 to 5^{12}.[1] The $5^{12}6^4$ and 5^{12} cages are from sII. The $5^{12}6^3$ cage was first reported by Vatamanu and Kusalik in crystalline and polycrystalline structures formed during the crystal growth of methane hydrates.[21] This type of cage has been observed in methane hydrate nucleation.[22,30] The small $4^3 5^6$ and $4^2 5^8$ cages are probably metastable and have not been previously reported to the best of our knowledge. Unlike

DOI: 10.1021/acs.jpcc.5b01869
J. Phys. Chem. C XXXX, XXX, XXX−XXX

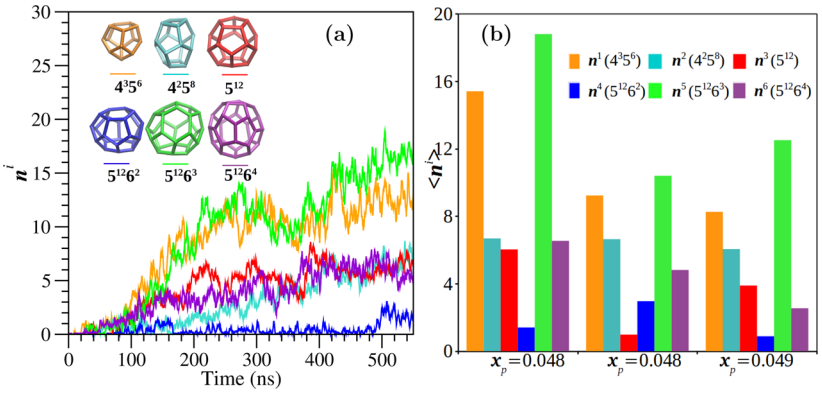

Figure 6. (a) Evolution of cage types in simulations for x_p = 0.048. The cages are represented by 4^l5^m and 5^m6^n where *l*, *m*, and *n* are, respectively, the number of square, pentagonal, and hexagonal faces forming the hydrate cages. The geometry of different cages is shown in the inset. The plots are produced by taking averages at intervals of 2 ns. (b) Average number of cages $\langle n^i \rangle$ computed over the last 50 ns of simulation time of three simulation runs. The plots and cages in (a) and the bars in (b) have the following color code: orange for 4^35^6; light blue for 4^25^8; red for 5^{12}; blue for $5^{12}6^2$; green for $5^{12}6^3$; and maroon for 5^{12} 6^4. T = 273.15 K and P = 500 bar.

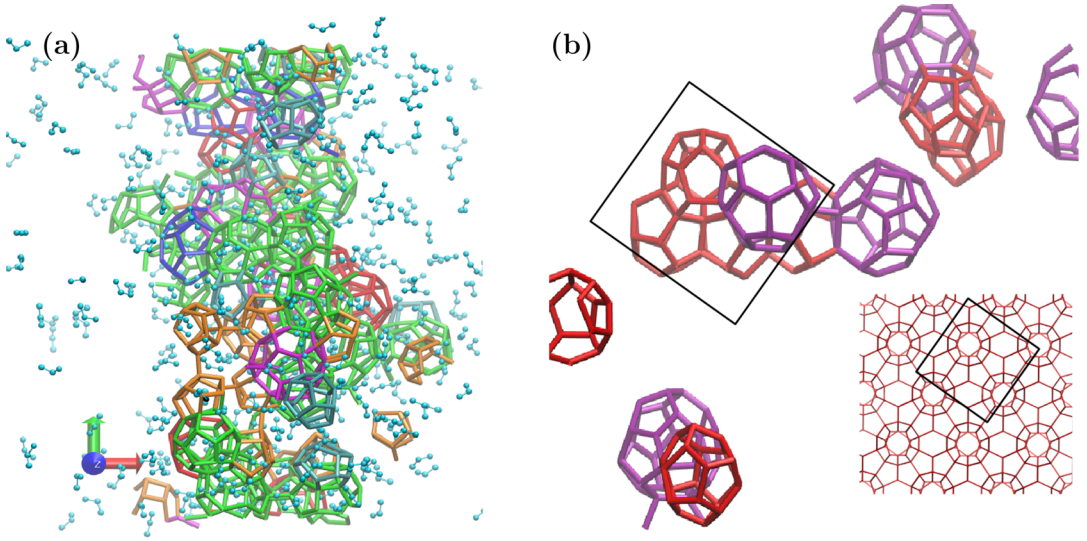

Figure 7. (a) Snapshot of the simulation box of setup D (Table S1 in the Supporting Information) showing hydrate cages at t = 550 ns. (b) sII motif found in seup D (boxed) and other 5^{12} and $5^{12}6^4$ cages. The cages are colored according to the color code in Figure 6. The inset shows the sII structure.[42] Propane molecules are colored in light blue. Free water molecules that do not form hydrate structures are not shown. x_p = 0.048, T = 273.15 K, and P = 500 bar.

methane which occupies 5^{12} cages,[14] in propane hydrate 5^{12} cages are empty.

Figure 6a shows the evolution of the number (n^i) of different types of cages formed in one of the two simulations for x_p = 0.048. Differently from N_S in Figure 5, here the cages may not be in the same cluster. Hydrate cages appear and disappear from the beginning and throughout the entire simulation. It is around $t \approx$ 48 ns that the first $5^{12}6^4$ cage forms and a sustained growth of the hydrate begins. At the same time the growth of the 4^35^6, and $5^{12}6^3$ cages initiates. These two types of cages are most abundantly formed at the end of the simulation. The growth of 5^{12} begins around $t \approx$ 90 ns and reaches a stable number at around $t \approx$ 400 ns, at the same time as the $5^{12}6^4$ cages. The formation of these cages is related to structure sII as we will see below. The small 4^25^8 cages appear and disappear at the first 100 ns of simulation. It is only at $t >$ 160 ns when they grow and reach a stable value at $t \approx$ 400 ns. Only few $5^{12}6^2$ cages (which are specific to sI) form during the 500 ns simulation.

The average number of cages formed in three different simulations is shown in Figure 6b. Two simulations are for x_p = 0.048 and the third one is for x_p = 0.049. In the three simulations the most abundant cage is $5^{12}6^3$ followed by the empty small 4^35^6, and 4^25^8 cages in third place. In one simulation for x_p = 0.048, the largest number of 5^{12} and $5^{12}6^4$ cages gives the largest amount of sII motifs. In the other simulation for x_p = 0.048, about four $5^{12}6^4$ cages and one 5^{12} cage form. The simulation for x_p = 0.049 has the lowest number of $5^{12}6^4$ cages. The number of $5^{12}6^2$ cages is the lowest in the three simulations.

The hydrate structure at the end of the simulation is mostly amorphous with motifs of sII. Figure 7a is a snapshot of the simulation box at the end of the simulation (t = 550 ns). Different types of cages are shown in the color code defined in Figure 6. It is clearly seen that the most abundant cages are $5^{12}6^3$ (green) and the 4^35^6 (orange). Figure 7b is a snapshot of a section of the simulation box of the same setup D (Table S1 in the Supporting Information), which shows only the sII motif and other 5^{12} and $5^{12}6^4$ cages. Propane forms sII at equilibrium,

DOI: 10.1021/acs.jpcc.5b01869
J. Phys. Chem. C XXXX, XXX, XXX−XXX

and our results are in line with the experiments.[43] At the lower temperature T = 270.15 K the same type of cages are found; however, motifs of structure sII are less likely to form.

CONCLUSIONS

Close to the limit of stability, nucleation time is significantly reduced in propane hydrate nucleation. At T = 273.15 nucleation is only accessible within a narrow concentration interval. At lower temperatures hydrate nucleation occurs in a wider range of conditions. We observe formation of motifs of structure II and two new 4^35^6 and 4^25^8 cages. Our results suggest that hydrate nucleation is prompted by high density fluctuations in the direction of fluid−fluid phase separation. In protein crystallization from solutions, accelerated nucleation is observed near the metastable liquid−liquid phase boundary.[15,16] The enhanced nucleation rate has been modeled by macromolecules interacting through a short-range attractive potential,[18,19] typically with a range ≤0.25 particles diameters. In this work we find that hydrate nucleation becomes remarkably fast in the vicinity of the fluid−fluid spinodal decomposition. Unlike others who use coarse-grain simulations,[17−19] we do not see a need to reduce potential interactions to capture hydrate nucleation in our atomistic model. We expect the accelerated nucleation to be a general process in fluid mixtures close to spinodal demixing with no restriction in their interaction potential.

ASSOCIATED CONTENT

Supporting Information

Table S1 (nucleation times of propane aqueous solu- tions at dierent conditions) and Figures SI and S2 (potential energy vs time, instantaneous size of the largest clusters during hydrate nucleation). This material is available free of charge via the Internet at http://pubs.acs.org

AUTHOR INFORMATION

Corresponding Author

*A. Firoozabadi. Phone: +1 (650)326-9172. Fax: +1 (650) 472-9285. E-mail: abbas.firoozabadi@yale.edu.

Notes

The authors declare no competing financial interest.

ACKNOWLEDGMENTS

We thank the member companies of the Reservoir Engineering Research Institute (RERI) for their financial support.

REFERENCES

(1) Sloan, E. D.; Koh, C. A. *Clathrate Hydrates of Natural Gases*; CRC Press: Boca Raton, FL, 2008.
(2) Buffett, B. A. Clathrate Hydrates. *Annu. Rev. Earth Planet. Sci.* **2000**, *28*, 477−507.
(3) Park, Y.; Kim, D.-Y.; Lee, J.-W.; Huh, D.-G.; Park, K.-P.; Lee, J.; Lee, H. Sequestering Carbon Dioxide into Complex Structures of Naturally Occurring Gas Hydrates. *Proc. Natl. Acad. Sci. U. S. A.* **2006**, *103*, 12690−12694.
(4) Chatti, I.; Delahaye, A.; Fournaison, L.; Petitet, J.-P. Benefits and Drawbacks of Clathrate Hydrates: A Review of Their Areas of Interest. *Energy Convers. Manage.* **2005**, *46*, 1333−1343.
(5) Glasby, G. Potential Impact on Climate of the Exploitation of Methane Hydrate Deposits Offshore. *Mar. Pet. Geol.* **2003**, *20*, 163−175.
(6) Florusse, L. J.; Peters, C. J.; Schoonman, J.; Hester, K. C.; Koh, C. A.; Dec, S. F.; Marsh, K. N.; Sloan, E. D. Stable Low-Pressure Hydrogen Clusters Stored in a Binary Clathrate Hydrate. *Science* **2004**, *306*, 469−471.
(7) Mao, W. L.; Mao, H.-K.; Goncharov, A. F.; Struzhkin, V. V.; Guo, Q.; Hu, J.; Shu, J.; Hemley, R. J.; Somayazulu, M.; Zhao, Y. Hydrogen Clusters in Clathrate Hydrate. *Science* **2002**, *297*, 2247−2249.
(8) Reagan, M. T.; Moridis, G. J. Global Climate and the Response of Oceanic Hydrate Accumulations. *Methane Hydrate Newsletter*; Earth Sciences Division, Lawrence Berkeley National Laboratory; Berkeley, CA, 2010; Vol. *10*, pp 9−12.
(9) Koh, C. A.; Sloan, E. D.; Sum, A. K.; Wu, D. T. Fundamentals and Applications of Gas Hydrates. *Annu. Rev. Chem. Bio. Eng.* **2011**, *27*, 237−257.
(10) Kashchiev, D.; Firoozabadi, A. Driving Force for Crystallization of Gas Hydrates. *J. Cryst. Growth* **2002**, *241*, 220−230.
(11) Kashchiev, D.; Firoozabadi, A. Nucleation of Gas Hydrates. *J. Cryst. Growth.* **2002**, *243*, 476−489.
(12) Vatamanu, J.; Kusalik, P. G. Observation of Two-Step Nucleation in Methane Hydrates. *Phys. Chem. Chem. Phys.* **2010**, *12*, 15065−15072.
(13) Liang, S.; Kusalik, P. G. Exploring Nucleation of H_2S Hydrates. *Chem. Sci.* **2011**, *2*, 1286−1292.
(14) Jiménez-Ángeles, F.; Firoozabadi, A. Nucleation of Methane Hydrates at Moderate Subcooling by Molecular Dynamics Simulations. *J. Phys. Chem. C* **2014**, *118*, 11310−11318.
(15) Galkin, O.; Vekilov, P. G. Control of Protein Crystal Nucleation around the Metastable Liquid-Liquid Phase Boundary. *Proteins* **2000**, *97*, 6277−6281.
(16) Vaiana, S. M.; Palma-Vittorelli, M. B.; Palma, M. U. Time Scale of Protein Aggregation Dictated by Liquid-Liquid Demixing. *Proteins* **2003**, *51*, 147.
(17) ten Wolde, P. R.; Frenkel, D. Enhancement of Protein Crystal Nucleation by Critical Density Fluctuations. *Science* **1997**, *277*, 1975−1977.
(18) Xu, L.; Buldyrev, S. V.; Stanley, H. E.; Franzese, G. Homogeneous Crystal Nucleation Near a Metastable Fluid-Fluid Phase Transition. *Phys. Rev. Lett.* **2012**, *109*, 095702.
(19) Talanquer, V.; Oxtoby, D. W. Crystal Nucleation in the Presence of a Metastable Critical Point. *J. Chem. Phys.* **1998**, *109*, 223−227.
(20) Moon, C.; Taylor, P. C.; Rodger, P. M. Molecular Dynamics Study of Gas Hydrate Formation. *J. Am. Chem. Soc.* **2003**, *125*, 4706−4707.
(21) Vatamanu, J.; Kusalik, P. G. Unusual Crystalline and Polycrystalline Structures in Methane Hydrates. *J. Am. Chem. Soc.* **2006**, *128*, 15588−15589.
(22) Walsh, M. R.; Koh, C. A.; Sloan, E. D.; Sum, A. K.; Wu, D. T. Microsecond Simulations of Spontaneous Methane Hydrate Nucleation and Growth. *Science* **2009**, *326*, 1095−1098.
(23) Jacobson, L. C.; Hujo, W.; Molinero, V. Thermodynamic Stability and Growth of Guest-Free Clathrate Hydrates. *J. Phys. Chem. B* **2009**, *113*, 10298−10307.
(24) Jacobson, L. C.; Hujo, W.; Molinero, V. Amorphous Precursors in the Nucleation of Clathrate Hydrates. *J. Am. Chem. Soc.* **2010**, *132*, 11806−11811.
(25) Jacobson, L. C.; Hujo, W.; Molinero, V. Nucleation Pathways of Clathrate Hydrates: Effect of Guest Size and Solubility. *J. Phys. Chem. B* **2010**, *132*, 13796−13807.
(26) Walsh, M. R.; Beckham, G. T.; Koh, C. A.; Sloan, E. D.; Wu, D. T.; Sum, A. K. Methane Hydrate Nucleation Rates from Molecular Dynamics Simulations: Effects of Aqueous Methane Concentration, Interfacial Curvature, and System Size. *J. Phys. Chem. C* **2011**, *115*, 21241−21248.
(27) Guo, G.-J.; Rodger, P. M. Solubility of Aqueous Methane Under Metastable Conditions. *J. Phys. Chem. B* **2013**, *117*, 6498−6504.
(28) Sarupria, S.; Debenedetti, P. G. Homogeneous Nucleation of Methane Hydrate in Microsecond Molecular Dynamics Simulations. *J. Phys. Chem. Lett.* **2012**, *3*, 2942−2947.

DOI: 10.1021/acs.jpcc.5b01869
J. Phys. Chem. C XXXX, XXX, XXX−XXX

(29) Zhang, J.; Guo, Y.; Yang, Y.; Kozielski, K. A Molecular Dynamic Study of Water/Methane/Propane. *J. Phys. B: At. Mol. Opt. Phys.* **2009**, *42*, 035302.
(30) Walsh, M. R.; Rainey, J. D.; Lafond, P. G.; Park, D.-H.; Beckham, G. T.; Jones, M. D.; Lee, K.-H.; Koh, C. A.; Sloan, E. D.; Wu, D. T.; Sum, A. K. The Cages, Dynamics, and Structuring of Incipient Methane Clathrate Hydrates. *Phys. Chem. Chem. Phys.* **2011**, *13*, 19951−19959.
(31) Abascal, J. L. F.; Sanz, E.; García Fernández, R.; Vega, C. A Potential Model for the Study of Ices and Amorphous Water: TIP4P/Ice. *J. Chem. Phys.* **2005**, *122*, 234511−1−9.
(32) Calero, S.; Dubbeldam, D.; Krishna, R.; Smit, B.; Vlugt, T. J. H.; Denayer, J. F. M.; Martens, J.; Maesen, T. L. M. Understanding the Role of Sodium During Adsorption: A Force Field for Alkanes in Sodium-Exchanged Faujasites. *J. Am. Chem. Soc.* **2004**, *126*, 11377−11386.
(33) Hess, B.; Kuttner, C.; van der Spoel, D.; Lindahl, E. GROMACS 4: Algorithms for Highly Efficient, Load-Balanced, and Scalable Molecular Simulation. *J. Chem. Theory Comput.* **2008**, *4*, 435−447.
(34) Firoozabadi, A. *Thermodynamics of Hydrocarbon Reservoirs*, 1st ed.; Mc Graw-Hill: New York, NY, 1999.
(35) Li, Z.; Firoozabadi, A. Cubic-Plus-Association (CPA) Equation of State for Water-Containing Mixtures: Is 'Cross Association' Necessary? *AIChE J.* **2009**, *55*, 1803.
(36) Tung, Y.-T.; Chen, L.-J.; Chen, Y.-P.; Lin, S.-T. The Growth of Structure I Methane Hydrate from Molecular Dynamics Simulations. *J. Phys. Chem. B* **2010**, *114*, 10804−10813.
(37) Jiménez-Ángeles, F.; Firoozabadi, A. Induced Charge Density and Thin Liquid Film at Hydrate/Methane Gas Interfaces. *J. Phys. Chem. C* **2014**, *118*, 26041−26048.
(38) Michalis, V. K.; Costandy, J.; Tsimpanogiannis, I. N.; Stubos, A. K.; Economou, I. G. Prediction of the Phase Equilibria of Methane Hydrates Using the Direct Phase Coexistence Methodology. *J. Chem. Phys.* **2015**, *142*, 0445011−04450112.
(39) Kobayashi, R.; Katz, D. Vapor-Liquid Equilibria For Binary Hydrocarbon-Water Systems. *Ind. & Eng. Chem.* **1953**, *45*, 440−446.
(40) Ballard, A. L.; Sloan, E. D. Hydrate Phase Diagrams for Methane + Ethane + Propane Mixtures. *Chem. Eng. Sci.* **2001**, *56*, 6883−6895.
(41) Sengers, J. V.; Sengers, J. M. H. L. In *Progress in Liquid Physics*; Croxton, C. A., Ed.; Critical Phenomena in Classical Fluids; John Wiley and Sons: Chichester, U.K., 1978; Chapter 4.
(42) Mark, T. C. W.; McMullan, R. K. Polyhedral Clathrate Hydrates. X. Structure of the Double Hydrate of Tetrahydrofuran and Hydrogen Sulfide. *J. Chem. Phys.* **1965**, *42*, 2732−2737.
(43) Rivera, J. J.; Janda, K. C. Ice Particle Size and Temperature Dependence of the Kinetics of Propane Clathrate Hydrate Formation. *J. Phys. Chem. C* **2012**, *116*, 19062−19072.

DOI: 10.1021/acs.jpcc.5b01869
J. Phys. Chem. C XXXX, XXX, XXX−XXX